Analyst

ROYAL SOCIETY OF CHEMISTRY

PAPER

View Article Online
View Journal | View Issue

Cite this: *Analyst*, 2025, **150**, 4059

Extension of microscale surface ion conduction (μSIC) to the sensing of charged small molecules: application to per- and poly-fluoroalkyl substances (PFASs)

Md Ruhul Amin, Beatrise Berzina, Umesha Peramune and Robbyn K. Anand *

Surface ion conduction-based sensing, which detects changes in ionic conductivity upon target binding, has been widely used for molecular detection. However, many sensors in this class, such as chemically modified solid-state nanopores, face challenges related to complex fabrication and inconsistent immobilization of target-specific probes at the nanoscale. In contrast, we previously introduced the microscale surface ion conduction (μSIC) sensor as a solution for detecting biological analytes. In this work, we demonstrate the adaptability of the μSIC sensor for organic pollutant detection, specifically targeting per- and polyfluoroalkyl substances (PFASs) in drinking and brackish waters. By integrating C18 reversed-phase silica gel chromatographic beads as a solid substrate, we enable label-free, non-optical detection of PFASs. This approach offers several advantages, including being labor-efficient, portable, and cost-effective, compared to conventional detection methods. By integrating an additional preconcentration step using faradaic ion concentration polarization (fICP) with a lateral flow assay (LFA) (fICP–LFA), the sensor's sensitivity was increased almost 77 times while the limit of detection (LOD) of perfluorooctane sulfonic acid (PFOS) was improved 1137-fold. It was also observed that the shift in current (signal) produced by the sensor does not change significantly over a range of background electrolyte (BGE) concentrations spanning three orders of magnitude. This work is significant as it implements a chromatographic solid phase as a substrate for label-free sensing, creating an avenue to develop a new class of sensors or to monitor chromatographic interactions. Further, we demonstrate that the μSIC sensor can be adopted for non-biological molecules, and to the best of our knowledge, this work is the first surface charge-based detection of PFASs.

Received 27th May 2025,
Accepted 5th August 2025

DOI: 10.1039/d5an00584a

rsc.li/analyst

1. Introduction

In this paper, we describe the quantification of perfluoroalkyl substances (PFASs), the so-called "forever chemicals" in water by microscale surface ion conduction (μSIC) – a non-optical, reagentless sensor – in the presence and absence of electrokinetic pre-enrichment of these analytes. Specifically, the accumulation of PFASs on a packed bed of C18 microbeads embedded in a microfluidic channel is measured through a change in the surface charge of the beads and a concomitant increase in the ionic conductivity of this porous bed. This advancement is significant for two reasons. First, this study is part of a broader exploration of factors that impact sensors for which transduction is accomplished *via* a change in ionic conductivity within microscale structures. The μSIC sensor has several distinct advantages relevant to point-of-need (PON) applications, such as ease of fabrication, simple electronics, and no need to add reagents. The μSIC has the potential to overcome limitations of its nanoscale counterparts with respect to ease of fabrication and flow-through operation, which supports rapid mass transfer. The present study examines the response of the μSIC sensor to charged small molecule analytes, where prior studies have focused on biomolecules and bioparticles.[1–3] Second, there is a need for methods to monitor PFASs in natural bodies of water and in drinking water at the PON. While in its current embodiment, the reported method lacks the sensitivity and selectivity required for these applications, this study provides a reference point that will inform subsequent optimization of the material and dimensions of the microbeads, and the extent of pre-enrichment needed to meet relevant performance metrics. The reported method is characterized by evaluating changes in the current–voltage characteristics of the μSIC sensor and zeta potential of the C18 microbeads that arise from the adsorption of two PFASs, perfluorooctane sulfonic acid

The Department of Chemistry, Iowa State University, 2415 Osborn Drive, 1605 Gilman Hall, Ames, Iowa 50011-1021, USA. E-mail: rkanand@iastate.edu

(PFOS) and perfluorobutane sulfonic acid (PFBS). We further evaluate signal enhancement *via* pre-enrichment of PFOS by counter-flow focusing facilitated by faradaic ion concentration polarization (fICP).

Sensors for which signal transduction is based on a change in the transport of charge carriers following analyte binding are among the most sensitive. These sensors can be further classified by the type of charge carrier – electrons/holes (*e.g.*, field-effect transistors (FETs)) and ions (*e.g.*, nanopore and membrane-based sensors). In a FET, source and drain electrical contacts are interconnected by a semiconducting gate, which for biological analytes, is modified with a bio-recognition agent. The binding of the analyte on or near the gate modulates the density of charge carriers (electrons or holes) in the conduction band, thereby changing the source-to-drain conductance, which is in turn detected as a change in the current measured in response to a voltage applied between the contacts.[4,5] In nanopore and nanoslit sensors, a probe is immobilized on the inner walls of the pore(s)[6] or slit(s),[7] and a voltage is applied across this nanoscale junction. Upon binding of target molecules, the distribution of charge within the electrical double layer (EDL) is modulated, and the ionic conductivity of these surfaces is altered as a result. This change is measured as an increase or decrease in current across the junction, and in the case of asymmetric pores, current rectification may result. Similarly, the binding of charged molecules on the surface of an ion exchange membrane (IEM) alters ion transport to the membrane, giving rise to a change in current.[6,8] For example, Senapati *et al*. have demonstrated a rapid, label-free nanoporous membrane-based biosensor for the selective detection of nucleic acids that utilizes ion concentration polarization (ICP) as the reporting mechanism.[8] They reported that due to the binding of negatively charged nucleic acids to an oligoprobe-modified membrane surface (a positively charged anion exchange membrane (AEM)), charge inversion of the membrane surface occurs. Due to this change of surface charge, ionic current transport through the nanoporous membrane changes, therefore altering the onset potential of the characteristic regimes of non-linear current–voltage curves. Despite the high sensitivity of all the techniques mentioned above, the remaining drawbacks are the complexity of device fabrication and probe immobilization. For example, in BioFETs, probe immobilization is performed *in situ* using either chemical (EDC/NHS coupling) or physical techniques (spin coating, plasma-enhanced chemical vapor deposition, deposition of functionalized gold nanoparticles).[9,10] These techniques can be time-consuming and often require access to clean room facilities. Further, the integration of enrichment protocols to increase the local concentration of analytes at the sensing interface is still an active area of research. Therefore, a surface-charged-based sensor that is easy to fabricate, supports facile immobilization of the target specific probes and is capable of on-chip analyte enrichment, is in high demand.

Our group has previously reported a surface charge-based microscale ion conduction (μSIC) sensor to detect biological analytes that addresses these challenges.[1,3] In the μSIC sensor, probe immobilization is carried out *ex situ* using commercially available substrates and straightforward probe immobilization protocols. The overall μSIC sensor design and working principle are demonstrated in Scheme 1a and b. The μSIC sensor comprises a microfluidic channel with two microbead beds that are in proximity: (i) a customizable bead bed onto which target-specific probes are immobilized (secondary bead bed) and (ii) a silver-coated glass bead bed (primary bead bed) working as a 3D electrode which is grounded. This device facilitates a lateral-flow assay (LFA) where the secondary bead bed functions as the test line. Upon binding of the target analyte on this test line, the surface charge and zeta potential of the bead's changes, and this change in turn alters the ionic conductivity across the secondary bed.[1,2] The magnitude of the change in conductivity (recorded as shift in current) corresponds to the logarithm of the target analyte concentration.

To improve the sensitivity and LOD of the μSIC sensor for low abundance analytes, we previously implemented electrokinetic enrichment facilitated by fICP.[1,3] In fICP, an electric potential is applied between the electrical leads (V^+) in the inlet and outlet *versus* the 3D electrode (ground, GND). Due to the application of this potential bias, faradaic reactions occurring at the 3D electrode generate an ion depletion zone (IDZ) *via* neutralization of ions of the background electrolyte (BGE). The key to the analyte enrichment is the formation of the low-conductivity (or highly resistive) IDZ. This low conductivity causes a localized augmentation of the electric field within the IDZ, resulting in a steep electric field gradient at the IDZ's boundary. This gradient can be leveraged for enrichment by counter-flow focusing – analytes enrich at an axial position where the electric field strength is sufficient to cause their convective and electromigratory velocities to be equal and opposite.[11,12] Moreover, the location of the enriched plug of analyte can be tuned to lie within the bed of probe modified beads, thus improving the equilibrium surface coverage. This pre-enrichment scheme is broadly applicable to a wide range of analytes. Using the μSIC sensor in combination with pre-enrichment, we have thus far demonstrated sensing of DNA (pM),[3] viral RNA (fM),[13] and antibodies (pM).[1] The relatively high sensitivity of the μSIC sensor for viral RNA (29 kb) and virus particles is attributed to the large size and high net charge of these analytes.

Here, we extend the application of the μSIC sensor to the detection of singly charged small molecules. We chose per- and polyfluoroalkyl substances (PFASs) as model target analytes. PFASs are a class of anthropogenic organic fluorinated compounds which can often be found in water, cause detrimental health effects and, therefore, need to be readily detected.[14,15] In this work, C18 beads were used for the secondary bead bed (target-binding). As both PFASs and C18 beads have hydrophobic moieties (long carbon chains), we anticipated hydrophobic interaction between PFASs and C18 beads which would give rise to a higher negative surface charge on C18 beads. Following the previous work,[1,3] we also anticipated that due to the increase of negative surface charge

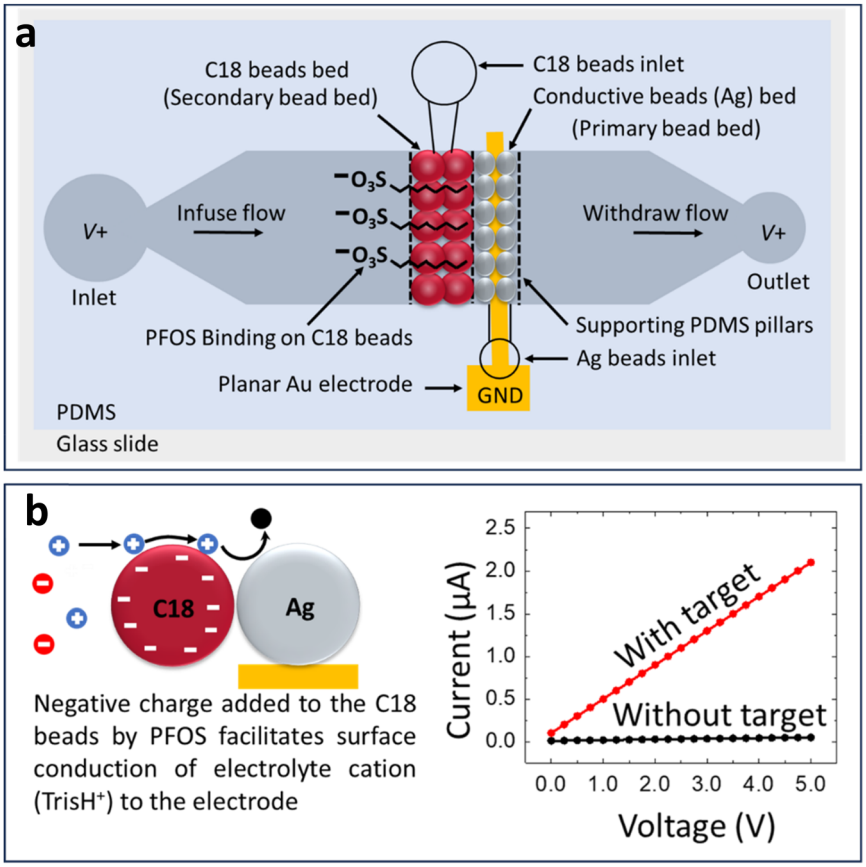

Scheme 1 (a) Illustration of overall device design (top view), (b) the suggested mechanism for enhanced system conductance due to PFOS adsorption on the C18 beads. An increase in the negative charge present on the C18 beads promotes surface conduction of cations to the conductive silver beads, resulting in a shift in current.

on beads, charge transport along their surfaces within the EDL would increase, as shown in Scheme 1b. It is important to note that C18 beads are not very specific towards PFASs. Yet, it proves the concept that binding of PFASs on chromatographic beads alters the bead surface charges, which can be determined as a change in current in the μSIC sensor. Moreover, we anticipate further improving the sensitivity and selectivity of the μSIC sensor by utilizing off-the-shelf beads with higher affinity to PFASs. Here, we observed that the shift in current increases with increasing PFOS concentration in both scenarios, with and without enrichment, which indicates the binding of PFASs on C18 beads. An LOD of 502.74 ppm and sensitivity of 0.96 μA mM^{-1} were obtained without enrichment. It was also observed that the signal increases with increasing length of the PFASs carbon chains indicating that both short and long-chain PFASs can be detected using μSIC sensor. Further, with the incorporation of fICP enrichment, LOD and sensitivity improved to 0.45 ppm (1117-fold improvement compared to LFA alone) and 73.89 μA mM^{-1} (77-fold compared to LFA), respectively. Lastly, we found that the signal produced by the sensor – the shift in current – changes minimally over a range of ionic strengths spanning three orders of magnitude.

This work is significant for several reasons. First, it differs from previous studies in that no target-specific probe is employed, and therefore, *ex situ* modification of the beads is not required – an unmodified, commercially available chromatographic extraction phase is employed. Second, the findings from this study are specifically relevant to sensing a critical environmental contaminant and broadly relevant to monitoring chromatographic interactions and detecting singly charged small molecules, which is important for separation science, and environmental and analytical chemistry. Finally, because the sensing platform is built entirely from commercially available materials, it enables rapid prototyping and mass production, which supports its application to water monitoring.

2. Experimental methods

2.1. Chemicals and reagents

Fluorescein dye was purchased from Acros Organics (Janssen-Pharmaceuticalaan 3 PB A 2440, Geel, Antwerp, Belgium). Perfluorobutane sulfonic acid (PFBS, 97% purity), HPLC grade C18 reverse-phase silica beads (particle size 15–25 μm, 100 Å pore size), chromium etchant, and AZ 400 K developer were

obtained from Sigma Aldrich (St Louis, MO). Perfluorooctane sulfonic acid (PFOS, 98% purity) was bought from AK Scientific (Union City, CA). Double-deionized distilled water (18.2 MΩ cm, Sartorius Arium Pro, Göttingen, Germany) was used to make all required solutions. Hollow glass microbeads coated with conductive silver (d = 10–20 μm, 0.67 g cc^{-1}) were purchased from Cospheric (Santa Barbara, CA). The devices were fabricated using poly(dimethylsiloxane) (PDMS) (Sylgard 184 elastomer kit, Dow Corning Corp., Midland, MI). Au-coated glass slides (1″ × 3″ × 0.40″, 1000 Å Au and 50 Å Cr adhesion layers) were used to fabricate patterned thin-film electrodes and were purchased from Evaporated Metal Films (Ithaca, NY).

2.2. Device design and fabrication

Standard photolithographic procedures were used for SU-8 silicon mold fabrication.[16] Briefly, the channel molds were prepared utilizing a negative photoresist (SU-8 2050, Microchem Corp., Westborough, MD) coated on Si substrate and wet-etched using SU-8 developer (Kayaku Advanced Materials, Westborough, MA). The etched wafer was silanized overnight using 1*H*,1*H*,2*H*,2*H*-perfluorooctyltrichlorosilane. Subsequently, replicas were formed by casting uncured PDMS on the SU-8 mold followed by curing at 65 °C for 24 h. Scheme 1a depicts the overall device design. The main channel's height, width, and length were 40 μm, 1.48 mm, and 11.0 mm, respectively. Two microbead beds, spanning the channel width, were located in the midpoint of the channel. These beds comprised silver-coated glass beads (primary) overlying a planar gold microband and C18 reversed-phase silica beads (secondary) upstream of the primary bead bed. The width (along the channel axis) of the primary and secondary bead beds were 300 μm and 500 μm, respectively. The beds were defined by PDMS pillars (20 μm wide) spaced 10 μm apart. The auxiliary channel for packing the Ag bead bed was 0.20 mm wide and 2.5 mm long. The auxiliary channel used for packing C18 beads was funnel-shaped with an opening width of 0.45 mm which narrowed down to 0.25 mm at the bead bed. The funnel-shaped channel was 1.0 mm long. A 1.0 mm-diameter biopsy punch was used to make the auxiliary channel inlets and main channel outlet, while a 3.0 mm-diameter biopsy punch was used for the main channel inlet.

The thin film Au microband electrode was fabricated on a glass slide following a previously reported technique, using a positive photoresist (AZ P4620, EMD Branchburg Plant, 70 Meister Avenue, Somerville NJ 08876).[17] The 200 μm-wide electrode was located at the middle of the main channel and was sufficiently long to span the channel width. A lead to the microband extended along the glass slide, beyond the PDMS monolith to a contact pad. The glass slide with patterned Au electrode and PDMS replica was exposed to air plasma (PDC-001, Harrick Plasma, Ithaca, NY) for 60 s, and then bonded together. To improve the strength of bonding, the assembled device was incubated at 65 °C for at least 18 h.

The conductive Ag-coated beads in DDI (5.0 μL, w/v = 22 mg mL^{-1}) were pipetted into the inlet to the packing channel for the primary bead bed, using negative pressure. Similary, C18 reversed-phase silica microbeads (approximately 5.0 μL, w/v = 20 mg mL^{-1}) were packed into the secondary bead bed, and then, both bead inlets were sealed using epoxy adhesive (double/bubble epoxy non-sag, Royal Adhesives & Sealants, LLC Wilmington, CA 90744). The inlet and outlet of each device were connected to a stainless-steel blunt needle (1.0 mm O.D.). These served as driving electrodes. The outlet needle was fitted with PTFE tubing and connected to the glass syringe (500 μL, Hamilton syringe) actuated by a syringe pump to control fluid flow.

2.3. Lateral flow assay (LFA) procedure

The devices were filled with Tris·$HClO_4$ buffer (100 mM, pH 8.35, unless specified otherwise for a subset of experiments) under negative pressure and rinsed for 20 min at 500 nL min^{-1}. Subsequently, the devices were conditioned by applying 3.0 V across the leads (V^+) at the inlet and outlet relative to the ground (GND) at the 3D Au/Ag electrode (Scheme 1a, primary bead bed) for 2.5 min, at 500 nL min^{-1}. This conditioning step was repeated twice, with a 1 min pause in between. Next, the flow rate was reduced to 100 nL min^{-1} for 10 min, at the end of which a current voltage curve (CVC) (0 to 5.0 V with 0.25 V increments at 0.33 s per step) was obtained. Three replicates were obtained with a 5 min increment in between measurements. The average of these replicates was used as the background current (i_{blank}). Then, the Tris·$HClO_4$ buffer in the device inlet was replaced with a working solution containing a distinct concentration of PFOS (0–2.0 mM PFOS) in 100 mM Tris·$HClO_4$. The flow rate was maintained at 100 nL min^{-1} for 30 min, and a CVC was obtained ($i_{analyte}$). The background current was subtracted from that obtained in the presence of PFOS to calculate the shift in current ($\Delta i = i_{analyte} - i_{blank}$). This shift was expected to arise from PFOS binding to the C18 beads. The shift in current was reported as a function of PFOS concentration and applied potential.

2.4. fICP focusing followed by LFA

In fICP–LFA experiments, following the conditioning step and acquisition of background CVCs (as described in subsection 2.3) for 10.0 mM Tris·$HClO_4$ buffer (pH 8.35), the buffer in the device inlet was replaced with a PFOS (0–0.50 mM) and fluorescein (100 μM) solution in Tris·$HClO_4$ (10 mM, pH 8.35). Then, the flow rate was reduced to 90 nL min^{-1} and allowed to stabilize for 10 min. Next, 7.0 V was applied between the leads in the inlet and outlet (V^+) *versus* ground (GND) at the 3D Au/Ag electrode for 30 min. Under these conditions, OH^- is generated *via* water reduction at the 3D electrode, which in turn neutralizes $TrisH^+$ to Tris. While alternative electrode materials are suitable to drive these reactions, Ag microbeads and a Au microband were selected due to their ready availability. To monitor the enrichment of fluorescein under this applied voltage, a Ti–S inverted fluorescence microscope (Nikon Industries, New York, NY) equipped with a camera (Orca Flash 4.0, Hamamatsu Corp, Bridgewater, NJ) was used. Following 30 min of enrichment, the device was flushed with the sample

solution at an increased flow rate of 100 nL min^{-1} for 10 min to remove all non-specifically bound species. Subsequently, another CVC was taken. The Δi was determined as described previously in the LFA procedure.

2.5. Zeta potential measurements

The zeta potential (ζ) of PFOS-adsorbed C18 beads was measured in 10 mM Tris·$HClO_4$ (pH 8.35) using a Zetasizer Nano ZS (Malvern, UK). Approximately 12.0 mg of C18 beads were incubated in 2.0 mL PFOS solution (10 mM Tris·$HClO_4$, pH 8.35) for 30 min. Then, the bead suspensions were centrifuged for 5 min at 7830 rpm, and the eluents were decanted. Further, the PFOS-adsorbed beads were resuspended and mixed well in 1.0 mL Tris·$HClO_4$ solution (10 mM, pH 8.35), and centrifuged for 2 min at 7830 rpm, and the eluent was discarded to remove any excess unbound PFOS. Finally, the PFOS-adsorbed beads were resuspended in 1.0 mL Tris·$HClO_4$ solution (10 mM, pH 8.35) and zeta potential (ζ) were measured. The average zeta potential ($\zeta_{average}$) of three replicates (n = 3) for each PFOS concentration is reported in Table 1.

3. Results and discussion

3.1. Zeta potential measurements

The zeta potential (ζ) is used as a physicochemical property to characterize ion adsorption and double-layer interactions between charged particles.[18] To investigate PFOS adsorption on C18 beads and the resulting change in surface charge, ζ measurements were conducted (more experimental details can be found in the Experimental methods section).

Table 1 shows the average zeta potential ($\zeta_{average}$) of C18 beads that were incubated with various PFOS concentrations (in 10 mM Tris·$HClO_4$, pH 8.35). Note that the $\zeta_{average}$ decreased from −21.93 mV (bare C18 microbeads) to −72.53 mV (for C18 microbeads incubated in 1.50 mM PFOS) and increased in magnitude with the logarithm of PFOS concentration. This increment of the magnitude of $\zeta_{average}$ demonstrates that the hydrophobic adsorption of PFOS on C18 microbeads leads to a substantial shift in microbead surface charge.[19] This shift is attributed to the negative SO_3^- functional group of the PFOS.

3.2. Non-optical detection of PFOS using LFA by surface ion conduction

Based on zeta potential measurement results, we evaluated whether hydrophobic adsorption of PFOS on C18 beads could lead to a change in the ionic conductivity through the bead bed. Previously, our group reported that the binding of charged analytes on the secondary bead (Scheme 1) surface changes the local ionic conductivity of the bead bed and leads to a change in ionic current which can be recorded at the 3D Au/Ag electrode (Scheme 1, primary bead bed).[1,3] Based on our ζ potential measurements (Table 1), we anticipated that the adsorption of negatively charged PFOS on C18 beads could alter the bead surface charge and the ion conduction along the bead surface.

To investigate PFOS adsorption *in situ* on the C18 bead surface, we first used an LFA with no fICP preconcentration step (more experimental details in the Experimental methods section). Fig. 1a shows the shift in CVC obtained for an LFA in the absence (blank) and presence of 1.5 mM PFOS in the sample solution (10 mM Tris·$HClO_4$). We observed a 1.60 μA shift in current (red trace) after 30 min of flowing the sample solution compared to the blank solution (no PFOS, black trace). This result indicates that the shift is attributable to adsorbed PFOS on the C18 beads and/or the contribution of dissolved PFOS to the conductivity of the bulk solution. To explore the influence of this solution-phase PFOS on the observed shift in current, we included a 10 min rinsing step in the LFA workflow to remove unbound species before obtaining the second set of CVCs. The rinsing time (minimum 6 min) was determined by considering the total volume of the channel (600 nL) and the rinsing-buffer flow rate (100 nL min^{-1}) to completely displace the sample solution. Fig. 1b shows the result of replicates in which the sample was rinsed from the channel for 10 min (with buffer only) prior to obtaining the second set of CVCs. This additional rinsing step was included to evaluate the contribution of solution-phase PFOS to the signal and potential desorption of PFOS from the C18 beads. After 10 min of rinsing, we observed a 0.57 μA shift in current for PFOS at 5.0 V (Fig. 1b, red trace) compared to the blank (black trace).

These results confirm that PFOS is adsorbing on C18 beads. Additionally, the decreased shift in current could possibly be due to (i) PFOS desorption from the C18 beads or/and (ii) removal of bulk PFOS, which could have contributed to the bulk conductance. Note that the latter contribution is significant only when the PFOS concentration is on the same order of magnitude as that of the electrolyte. This potential source of error can be addressed by the introduction of a rinsing step, by increasing the electrolyte concentration, or by correcting for the conductivity of the sample. Another notable feature of the results shown in Fig. 1 is that the addition of a rinsing step reduces the standard deviation of the signal obtained for samples containing PFOS by 76% (at 5.0 V).

To avoid the desorption of adsorbed PFOS and to reduce the possible contribution from bulk conductivity, a 5 min rinsing period with background buffer was added to the LFA (experimental details are in the SI). We measured the shift in current obtained prior to sample introduction to after added final rinsing step. Fig. S1a is a plot of corresponding shift in current as a function of applied voltage obtained for several

Table 1 Zeta potential of C18 beads in Tris·$HClO_4$ (10 mM, pH 8.35) after incubation with PFOS

[PFOS] (mM)	Zeta potential (mV)	Conductivity (mS cm^{-1})
0.00	−21.93 (±3.01)	0.374 (±0.009)
0.50	−60.97 (±1.68)	0.379 (±0.007)
1.00	−64.90 (±2.04)	0.393 (±0.004)
1.50	−72.53 (±2.47)	0.384 (±0.007)

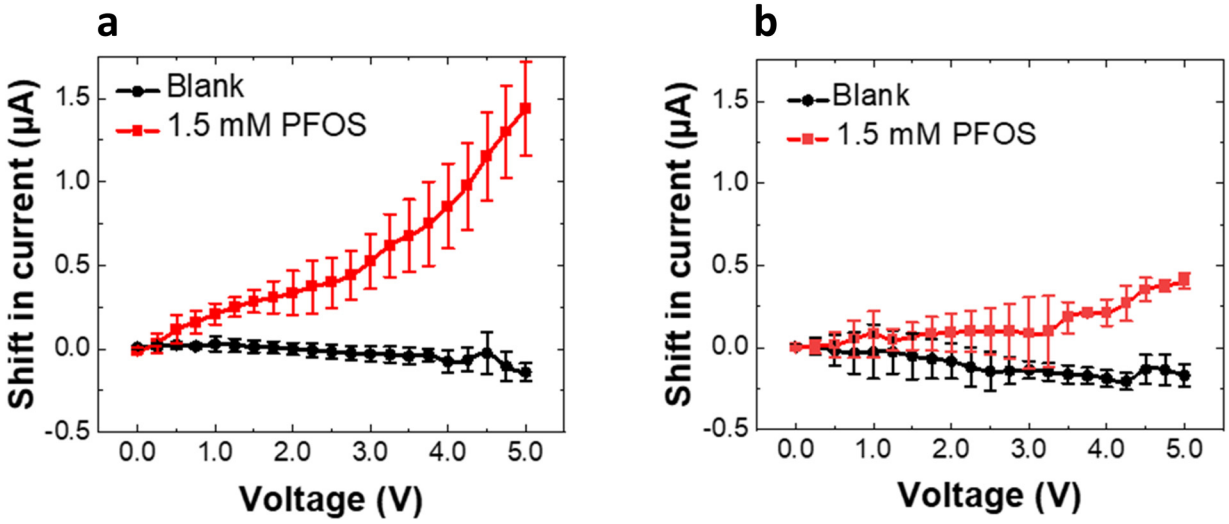

Fig. 1 Plots demonstrating the shift in current as a function of voltage for the adsorption of 1.5 mM PFOS on C18 beads in 10 mM Tris·$HClO_4$ (pH 8.35) (a) after 30 min of PFOS flowing (0 mM black trace, 1.5 mM red trace, $n \geq 3$) and (b) after 10 min of rinsing (after PFOS flowing) with background electrolyte solution (0 mM black trace, 1.5 mM red trace, $n \geq 3$).

distinct PFOS concentrations (0–2.0 mM). The observed upward trend in the shift in current implies that the electrical conductivity of the system is augmented with increasing PFOS concentrations. The increased electrical conductivity is attributed to enhanced surface conduction caused by greater negative surface charge on the C18 beads due to the sulfonate group of PFOS. Fig. S1b is a calibration curve depicting the relationship between the PFOS concentration and the shift in current at 5.0 V. The shift in current is linearly proportional to the PFOS concentration. Accordingly, the LOD of this LFA with the rinsing step is 648 ppm. The LOD was calculated from the linear fit of the calibration curve to determine the PFOS concentration corresponding to the blank + 3SD (i_{blank} + 3SD, $n \geq 3$, without PFOS). The sensitivity of the LFA is 0.67 μA/mM (slope (κ) of the calibration curve). Due to the surface charge-based sensing mechanism, a key design criterion is achieving a strong contrast in the bead's zeta potential before and after analyte binding. pH also plays a critical role in signal behavior. The target analyte in this study, PFOS, has a very low pK_a and is therefore expected to remain negatively charged across a wide pH range. Similarly, the C18 bead surface remains neutral across these conditions. In contrast, when either the analyte (*e.g.*, perfluorooctanoic acid, PFOA) or the bead has a moderate pK_a, the net surface charge, and thus the signal, can vary with pH.

To reduce the experimental time and exclude the rinsing step, we decreased the analyte/electrolyte concentration ratio, assuming that at higher electrolyte concentration, the impact of bulk PFOS conductivity would be negligible. To explore this assumption, we measured the shift in current for distinct concentrations of PFOS (0–2.0 mM) in 100 mM Tris·$HClO_4$ using the LFA (more details are included in the Experimental methods section). Similar to the LFA with the rinsing step result, Fig. 2a and b show that with increasing PFOS concentration, the shift in current increases and that the relationship is linear. The LOD and sensitivity were 502.74 ppm and 0.96 μA mM^{-1}, respectively. By comparing the LODs of the LFAs with and without a rinsing step, it is clear that when the analyte-to-electrolyte ratio is small, the contribution from the bulk PFOS conductivity to the shift in current is negligible.

The capability of detecting short-chain (4-carbon backbone) and long-chain (8-carbon backbone) PFASs is essential as both cause similar detrimental health effects. We investigated the impact of chain length on our sensor's performance. Fig. 3 demonstrates a shift in current for PFBS (1.50 mM, 4-carbon backbone, red trace) and PFOS (1.50 mM, 8-carbon backbone, blue trace) in 10 mM Tris·$HClO_4$ (pH 8.35).

The shift in current (1.50 μA) for PFOS is 3 times higher compared to PFBS (0.53 μA) at 5 V. This result indicates that the longer the carbon chain, the higher is the affinity of PFASs to C18 beads due to the larger hydrophobic surface area, and most importantly, this affinity results in a higher signal.[15] Moreover, shorter carbon chain PFASs are more hydrophilic compared to longer carbon chains that might cause weaker binding affinity with hydrophobic C18 beads.[20] This result supports our claim that the signal (shift in current) arises from the adsorption of these PFASs on the C18 beads. Based on these findings, we anticipate that the μSIC sensor with a packed bed of C18 beads is suitable for the detection of PFASs with various carbon backbone chain lengths.

The preceding experiments provide a proof-of-concept that the μSIC sensor can be utilized for singly-charged small molecule analytes. However, the hydrophobic interaction of C18 with PFASs is non-specific, and the calculated LODs are 6–8 orders of magnitude above relevant ranges for environmental samples or drinking water (parts per trillion). Several approaches can be used to improve the performance of the

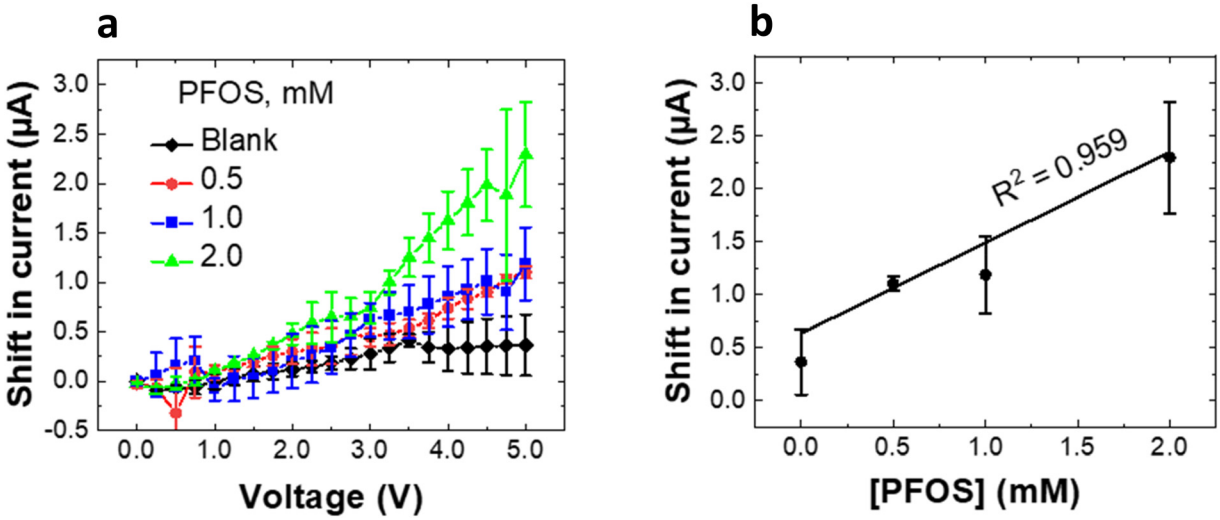

Fig. 2 All CVCs were taken after 30 min of PFOS flowing in 100 mM Tris·$HClO_4$ (pH 8.35) with on-chip LFA. (a) A plot of CVC shifts for a series of PFOS concentrations (0 mM black, 0.5 mM red, 1.0 mM blue, 2.0 mM green). (b) Calibration curve obtained for the on-chip LFA ($n \geq 3$) at 5 V and t = 30 min.

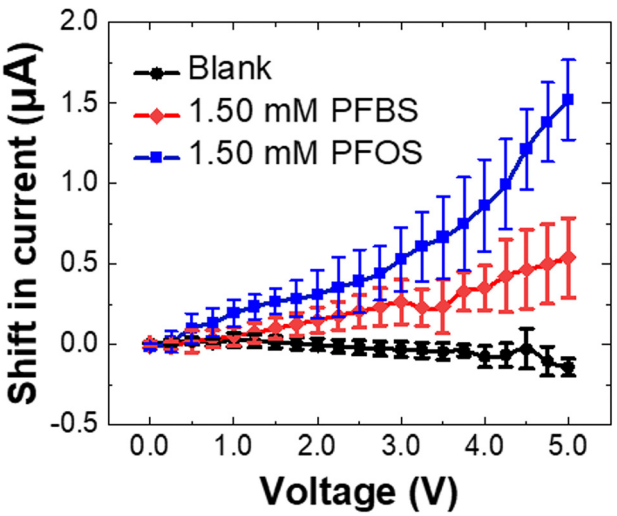

Fig. 3 Plot showing the CVC shift for blank (10 mM Tris·$HClO_4$, black) PFBS (4 carbons, red), and PFOS (8 carbons, blue) in 10 mM Tris·$HClO_4$ (pH 8.35) ($n \geq 3$).

μSIC sensor for the detection of PFASs. First, modifying the bead surface with molecules that have a higher affinity for PFASs can add specificity, and second, integration of this LFA with preconcentration methods can increase sensitivity. We further investigated the possibility of improving the LOD by preconcentrating PFOS using an electrokinetic technique, specifically fICP integrated with the LFA, as discussed in the following subsection.

3.3. Integration of fICP enrichment with LFA

To improve the LOD of the sensor, we incorporated an fICP focusing step in the LFA workflow. ICP and fICP have the ability to generate a focused plug of a charged small molecule analyte that is up to 9 orders of magnitude greater than that present in the input sample stream. This degree of preconcentration requires long enrichment times (several hours) and/or hierarchical fluidic networks coupled with multistage enrichment. As a preliminary investigation of the interplay of fICP with μSIC for PFASs sensing, we employed a 30 min single step of enrichment, which increases local PFOS concentration by 1–2 orders of magnitude. Fig. 4 demonstrates the fICP mechanism and how it is used for PFOS preconcentration in our system. Briefly, the microchannel with in-line 3D (Au/Ag) electrode is filled with background electrolyte solution (10 mM Tris·$HClO_4$, pH 8.35), and constant flow is established (left to right, Fig. 4). Further, the voltage is applied between the driving electrodes (V^+, anode) and ground (GND, cathode) (Fig. 4a). When voltage is applied, water is reduced at the cathode, and hydroxide (OH^-) is generated. An OH^- ion then accepts a proton from $TrisH^+$ (cation from the background electrolyte) to produce a neutral species (Tris). This process leads to the local depletion of electrolyte ions and the formation of an IDZ. Due to the low conductivity and high resistivity of the IDZ, a steep electric field gradient forms at the IDZ boundary (Fig. 4b). This gradient plays an important role in the focusing of charged analytes – in the presence of fluid flow, a charged analyte (*e.g.*, PFOS) focuses at a distinct axial location where its convective and electromigratory velocities are equal and opposite.[2,21] Fig. 4c is a brightfield micrograph of the central segment of the microchannel (top view), in which there are three rows of retention pillars that define the two bead beds; the right-side bed (downstream) is packed with conductive Ag-coated microbeads overlaying a thin-film Au microband, and the left-side bed (upstream) is packed with C18 beads. Here, fluorescein dye (100 μM) was used as a model analyte to visualize the location of the IDZ boundary in

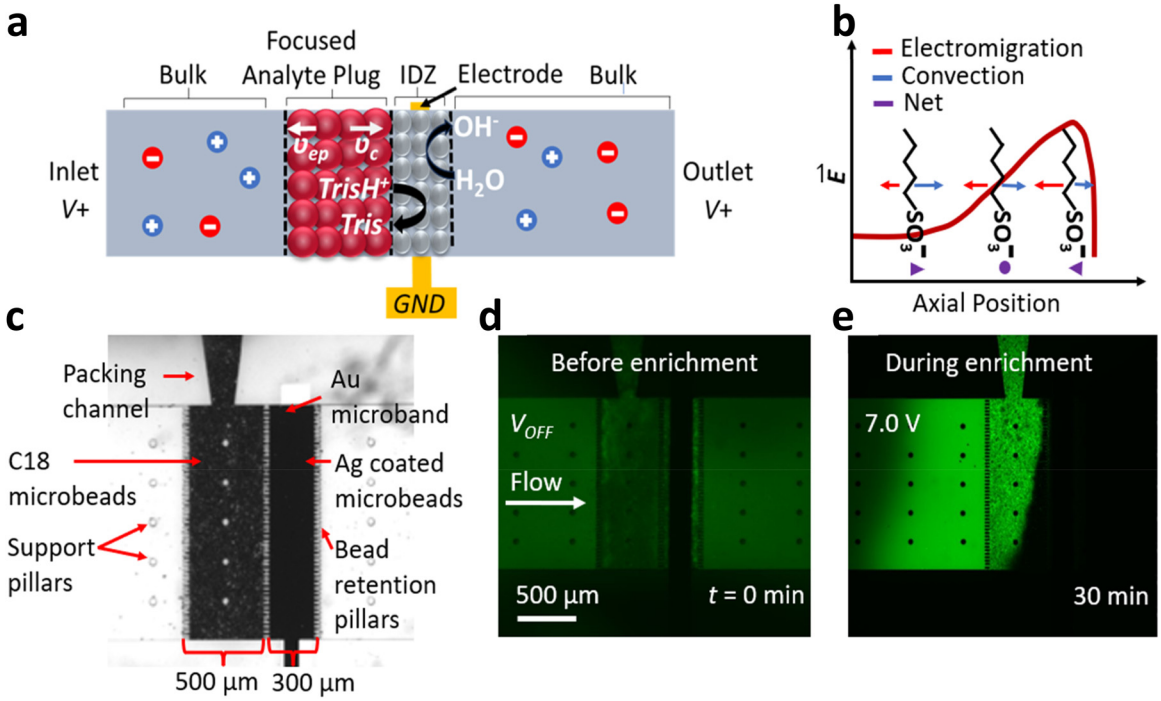

Fig. 4 (a) Schematic showing the mechanism of fICP. (b) Demonstration of the focusing of PFOS within an electric field gradient, especially at the interface of the IDZ in the presence of convection. (c) Brightfield micrograph of C18 and Ag bead beds located at the center of the microchannel. (d and e) Fluorescence micrographs of the enrichment of 100 μM fluorescein dye in 10 mM Tris·$HClO_4$ under an applied voltage of V^+ = 7.0 V at t = 0 and 30 min.

the microfluidic channel and extent of enrichment achieved by fICP. Fig. 4d and e are fluorescence micrographs that show the distribution of fluorescein in the microfluidic channel before and during the application of voltage for fICP (in the absence of PFASs). 26.5-Fold enrichment of fluorescein was obtained within 30 min of application of the voltage. A detailed description of the equipment and procedure used for fICP, imaging, and calculation of enrichment factor (EF) are included in the SI. Since the EF is largely determined by the rate of delivery of the analyte to the plug and the steepness of the electric field gradient, it is anticipated that a similar EF would be obtained for PFOS. The enrichment was limited by the requirements of electroneutrality – if the local concentration of fluorescein approaches that of the BGE, then its enrichment plateaus and the enriched analyte plug simply broadens with time.[22,23]

Having established the conditions for enrichment, we next confirmed that fluorescein would not influence PFOS detection during a LFA enhanced by fICP. The detailed procedure for the combined fICP–LFA method is provided in the more details are included in the Experimental methods section. Fig. 5a is a plot of the shift in current as a function of voltage obtained for 10 mM Tris·$HClO_4$ only ("Blank", black trace) and also for 100 μM fluorescein in 10 mM Tris·$HClO_4$ ("Fluorescein", red trace) using the fICP–LFA approach. As shown in Fig. 5a, there was no significant shift in current between the two cases, thus confirming that fluorescein does not increase the current either *via* adsorption on the C18 beads or by undergoing faradaic reactions.

Then, we compared the shift in current with and without enrichment for 0.01 mM PFOS in a solution of 10 mM Tris·$HClO_4$ and 100 μM fluorescein dye. Fig. 5b shows a 0.8 μA shift in current with enrichment (fICP–LFA, red trace) compared to without enrichment (LFA only, black trace). Next, we calculated the shifts in current for a series of PFOS concentrations (0.005–0.5 mM) following fICP-driven preconcentration (Fig. 5c). As previously in LFA, we observed shifts in current increased with increasing starting concentration of PFOS. Notably, the lowest detectable PFOS concentration for LFA method was 200 μM whereas for fICP–LFA approach, it was 5.0 μM in 10 mM Tris·$HClO_4$ (Fig. S3). We then plotted the shift in current at 5.0 V as a function of concentration to obtain a calibration curve for fICP–LFA (Fig. 5d). The calibration curve was fitted to the Langmuir adsorption isotherms with R^2 value of 1.00, indicating a good correlation between predicted and experimental values. In PFOS concentrations higher than 0.15 mM, the shift in current reached a plateau, which may be caused by the saturation of the bead bed surface with PFOS and/or secondary micelle/hemimicelle formation.[19] We applied linear fitting to the linear portion of the curve to obtain the LOD of fICP–LFA. The LOD of fICP–LFA was 0.45 ppm, a 1117-fold improvement in LOD, and a 77-fold improvement in sensitivity when compared to the LFA. The fICP–LFA sensitivity determined using the linear part of the calibration curve is 73.89 μA mM^{-1} (slope (κ) of the linear part of the calibration plot).

We anticipate that molecules that have higher charge density would further facilitate surface conduction and

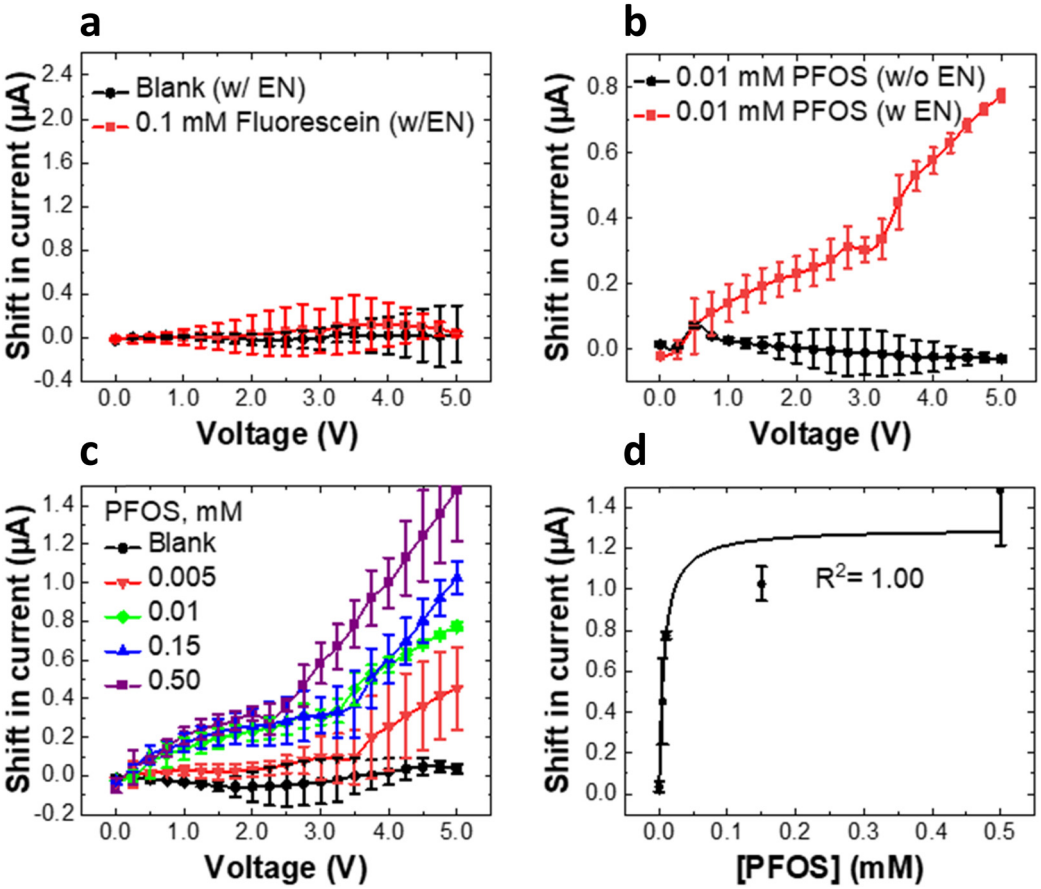

Fig. 5 fICP enrichment (EN) of PFOS at 7.0 V for 30 min directly over the C18 bead bed followed by CVCs from 0–5.0 V ($n \geq 3$). (a) A plot of CVC shifts after electrokinetic enrichment of blank (only Tris·$HClO_4$) and 0.1 mM fluorescein dye in 10 mM Tris·$HClO_4$. (b) A plot showing the CVC shift with and without enrichment of 0.01 mM PFOS (in a mixture of 0.1 mM fluorescein and 10 mM Tris·$HClO_4$). (c) A plot of the shift in current as a function of voltage for five distinct concentrations of PFOS (0 Mm black, 0.005 red, 0.01 green, 0.15 blue, 0.50 mM purple) was obtained after electrokinetic enrichment. (d) Calibration curve generated for the fICP–LFA and fitted to Langmuir adsorption isotherms.

enhance the sensitivity of the μSIC. From previous work in our group, we have observed that the sensitivity of the μSIC sensor is higher for larger analytes that are multiply charged such as rabbit IgG (15 mA mM^{-1})[1] compared to smaller and singly charged molecules like PFOS.

As a control, we investigated the impact of fICP conditions (30 min at 7.0 V) on the device itself. Fig. S2 shows the shift in CVC obtained in the absence of pre-enrichment for LFAs carried out for 0.15 mM PFOS (10 mM Tris·$HClO_4$) in two devices – one that had previously been exposed to fICP conditions (red trace) and one that had not (black trace). The shift in current was 7.5 times greater (at 5.0 V) for the device subjected to fICP conditions. Further, fICP-based enrichment of PFOS prior to the LFA produced a still greater shift in current (blue trace). These results indicate that fICP conditions sensitize the electrode and that this sensitization accounts for nearly 34% of the observed signal enhancement. Overall, these results indicate that fICP both sensitizes the electrode and increases the local concentration of PFOS within the C18 bead bed. These results reveal the dual mechanism by which fICP enhances the sensitivity of the μSIC sensor. Practical implications of this finding are: (1) device pre-treatment alone may achieve the requisite sensitivity for certain applications and obviate the need for a pre-enrichment step carried out by the end user, and (2) calibration curves obtained for this sensor in the absence and presence of fICP are not linearly related by the EF (*e.g.*, for EF = 25, the signal obtained for 0.01 mM PFOS is not the same as that given by 0.25 mM PFOS without enrichment).

3.4. Impact of background electrolyte concentration

To investigate the impact of the ionic strength of the sample matrix on the performance of the μSIC sensor, the shift in current was measured using the LFA method (without fICP enrichment) for a fixed concentration of PFOS (1.5 mM) in several distinct concentrations of BGE (0.1, 1.0, 10, and 100 mM Tris·$HClO_4$, pH 8.35). These concentrations were chosen to represent fresh (salinity <17 mM) and brackish (salinity is between 17–427 mM) waters.[24] Here, the background current was first measured for a specific concentration of BGE, followed by the introduction of PFOS solution in the same BGE. At all BGE concentrations, the shift in current that

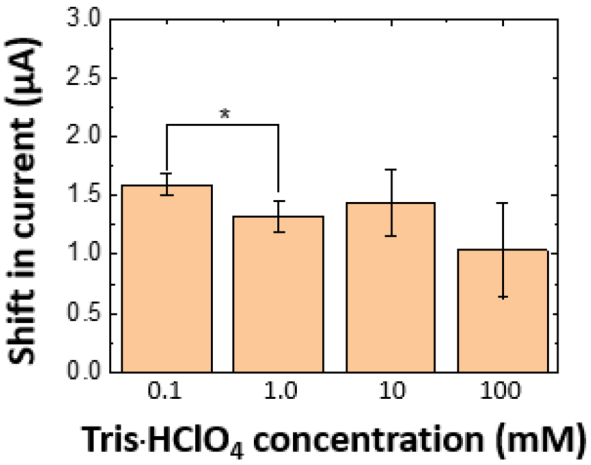

Fig. 6 Signal (shift in current) produced with lateral flow assay (without enrichment) after binding of 1.5 mM PFOS on C18 beads in distinct concentrations of Tris·$HClO_4$ at pH 8.35 ($n \geq 3$).

resulted from PFOS adsorption was measured at 5.0 V because the S/N ratio was highest at this voltage (Table S2). Fig. 6 shows the shift in current as a function of Tris·$HClO_4$ concentration. We observed that between the lowest two BGE concentrations (0.1 and 1.0 mM), the shift in current decreased by about 16% ($p < 0.05$, Table S3). This result suggests that, within this lower BGE concentration range, the sensor's signal does not remain constant but instead increases with decreasing ionic strength. This behavior can be attributed to a decrease in the thickness of the EDL, which reduces its screening capacity. As the EDL becomes less effective at shielding surface charges, ion conduction becomes more sensitive to changes in surface charge, thereby decreasing the sensor's sensitivity. However, at higher BGE concentrations (>1.0 mM Tris·$HClO_4$), the shift in current no longer significantly depended on ionic strength.

This finding agrees with the previous reports that zeta potential becomes independent of ionic strength at higher ionic strength BGE.[25,26] Vinogradov *et al*. explained that at low ionic strength, ion density in the diffuse EDL follows Boltzmann-like behavior, with weak screening of surface charge. At higher ionic strengths, ion-ion interactions in the bulk solution dominate, effectively screening the surface charge and reducing its influence on ion conduction.[25] Further, it is also noteworthy that the signal-to-noise ratio nearly doubles with each order of magnitude increase in ionic strength (Table S2), and this in turn worsens the LOD.

4. Conclusions

Here, we have demonstrated the application of the μSIC sensor for the detection of PFASs in brackish (1–100 mM ionic strength) and fresh water (~0.1 mM). We have demonstrated that these singly-charged small molecules can be detected by a simple LFA in this device, with a sensitivity of 0.96 μA mM^{-1} and an LOD of 502.74 ppm in the absence of preconcentration. In this LFA, the test line comprises C18 microbeads, and the readout is based on an increase in ionic conductivity of the surface of these beads upon adsorption of PFASs (PFOS or PFBS). By adding an electrokinetic preconcentration step (by fICP focusing), the sensitivity (73.89 μA mM^{-1}) and LOD (0.45 ppm) are enhanced in comparison to the LFA. This enhancement is attributable to both localized enrichment of the target analyte and sensitization (activation) of the electrodes. Furthermore, our results demonstrate that the signal (shift in current) varies significantly at lower BGE concentrations but does not vary significantly at higher BGE concentrations (>1 mM), which aligns with other available surface charge-based sensors. Importantly, the presented platform is low-cost (<$20), non-optical, label- and reagent-free. The sensor is capable of continuous monitoring of a flowing sample – an operating mode that we are currently investigating. We envision its use for on-site monitoring of PFASs, which is a considerable advancement to PFASs sensing compared to current instrument-based techniques. Selectivity of the μSIC sensor can be improved by using materials with a higher specificity for PFASs while the LOD can be further improved by optimizing experimental parameters used for enrichment and sensing (*e.g.*, bead affinity for PFASs, bead diameter, bead bed dimensions, longer duration or multistage enrichment).

Author contributions

Md Ruhul Amin: Conceptualization, methodology, formal analysis, investigation, visualization, writing – original draft. Beatrise Berzina: Supervision, conceptualization, writing – review & editing. Umesha Peramune: Methodology. Robbyn K. Anand: Supervision, conceptualization, writing – review & editing.

Conflicts of interest

Authors declare no competing interest.

Data availability

A subset of data may be included as SI within the manuscript. For further data access, please contact the corresponding author. The SI contains the procedure and result for an LFA with a rinsing step, the methods employed for fluorescence imaging and data processing, control experiments evaluating the impact of the conditions (*i.e.*, applied voltage) employed for enrichment on the electrodes and device performance, and statistical analysis of the impact of electrolyte concentration on the signal-to-noise ratio of the sensor.

Supplementary information is available. See DOI: **https://doi.org/10.1039/d5an00584a**.

Acknowledgements

This work was supported by an NSF CAREER grant awarded by the Chemistry Directorate Chemical Measurement and Imaging Program under award number 1849109. Additionally, this work was supported by the National Science Foundation Convergence Accelerator Program under Grant No. 2344398.

References

1 S. Osman, E. L. Claus and R. K. Anand, *Anal. Chem.*, 2023, **95**, 9337–9346.
2 B. Berzina, S. Kim, U. Peramune, K. Saurabh, B. Ganapathysubramanian and R. K. Anand, *Lab-on-a-Chip*, 2022, **22**, 573–583.
3 B. Berzina, U. Peramune, S. Kim, K. Saurabh, E. L. Claus, M. E. Strait, B. Ganapathysubramanian and R. K. Anand, *ACS Sens.*, 2023, **8**, 1173–1182.
4 D. Shahdeo, N. Chauhan, A. Majumdar, A. Ghosh and S. Gandhi, *ACS Appl. Bio Mater.*, 2022, **5**, 3563–3572.
5 D. Sadighbayan, M. Hasanzadeh and E. Ghafar-Zadeh, *TrAC, Trends Anal. Chem.*, 2020, **133**, 116067.
6 K. L. Rahn, U. Peramune, T. Zhang and R. K. Anand, *Annu. Rev. Anal. Chem.*, 2023, **16**, 49–69.
7 Y. Liu and L. Yobas, *Nano Lett.*, 2014, **14**, 6983–6990.
8 S. Senapati, Z. Slouka, S. S. Shah, S. K. Behura, Z. Shi, M. S. Stack, D. W. Severson and H.-C. Chang, *Biosens. Bioelectron.*, 2014, **60**, 92–100.
9 R. Hao, L. Liu, J. Yuan, L. Wu and S. Lei, *Biosensors*, 2023, **13**, 426.
10 N. Nakatsuka, K.-A. Yang, J. M. Abendroth, K. M. Cheung, X. Xu, H. Yang, C. Zhao, B. Zhu, Y. S. Rim, Y. Yang, P. S. Weiss, M. N. Stojanović and A. M. Andrews, *Science*, 2018, **362**, 319–324.
11 M. Li and R. K. Anand, *Analyst*, 2016, **141**, 3496–3510.
12 B. Berzina and R. K. Anand, *Anal. Chim. Acta*, 2020, **1128**, 149–173.
13 S. U. Devasinghe, E. L. Claus, M. E. Strait, D. Pagariya and R. K. Anand, *ACS Sens.*, 2024, **9**, 5776–5781.
14 Y. Wang, S. B. Darling and J. Chen, *ACS Appl. Mater. Interfaces*, 2021, **13**, 60789–60814.
15 D. Q. Zhang, W. L. Zhang and Y. N. Liang, *Sci. Total Environ.*, 2019, **694**, 133606.
16 J. C. McDonald and G. M. Whitesides, *Acc. Chem. Res.*, 2002, **35**, 491–499.
17 Y. Xia and G. M. Whitesides, *Annu. Rev. Mater. Sci.*, 1998, **28**, 153–184.
18 P. Leroy, N. Devau, A. Revil and M. Bizi, *J. Colloid Interface Sci.*, 2013, **410**, 81–93.
19 Z. Du, S. Deng, Y. Bei, Q. Huang, B. Wang, J. Huang and G. Yu, *J. Hazard. Mater.*, 2014, **274**, 443–454.
20 A. R. Santiago, S. Yin, J. Elbert, J. Lee, D. Shukla and X. Su, *J. Am. Chem. Soc.*, 2023, **145**, 9508–9519.
21 J. Choi, K. Huh, D. J. Moon, H. Lee, S. Y. Son, K. Kim, H. C. Kim, J.-H. Chae, G. Y. Sung, H.-Y. Kim, J. W. Hong and S. J. Kim, *RSC Adv.*, 2015, **5**, 66178–66184.
22 V. A. Papadimitriou, L. I. Segerink and J. C. T. Eijkel, *Anal. Chem.*, 2020, **92**, 4866–4874.
23 W. Ouyang, X. Ye, Z. Li and J. Han, *Nanoscale*, 2018, **10**, 15187–15194.
24 J. R. Du, X. Zhang, X. Feng, Y. Wu, F. Cheng and M. E. A. Ali, *Desalination*, 2020, **491**, 114445.
25 J. Vinogradov, M. D. Jackson and M. Chamerois, *Colloids Surf., A*, 2018, **553**, 259–271.
26 M. Z. Jaafar, J. Vinogradov and M. D. Jackson, *Geophys. Res. Lett.*, 2009, **36**, L21306.